

# Millimeter-Wave Frequency-Diverse Imaging with Phased Array Intended for Communications

Mikko K. Leino<sup>\*</sup>, Jan Bergman, Juha Ala-Laurinaho, and Ville Viikari

**Abstract**—This paper presents a recent progress in a millimeter-wave imaging done with a potential 5G base-station phased-array antenna exhibiting frequency-diverse, non-focused beams. The presented imaging system operates in 24–32 GHz band and is the first realization where phased arrays primarily developed for 5G communications are utilized in a frequency-diverse imaging application. The image reconstruction method solves the linear inverse problem with an iterative algorithm, and several images have been reconstructed based on the measurement data. Currently, a metallic sphere can be successfully located in the target space. However, future work is still required, and the paper further discusses the possibilities and restrictions of the current imaging setup.

## 1. INTRODUCTION

Millimeter-wave (mm-wave) phased arrays designed for 5G networks can serve other needs as well in addition to communications. For example, the state-of-the-art radar systems also utilize phased arrays [1–3], and thus, have similar operation principles to the upcoming 5G antennas presented, e.g., in [4–6]. Millimeter-wave frequencies are also suitable for imaging purposes, since the small wavelength enables higher spatial resolution in the image reconstruction.

Communication antennas meant for mm-wave 5G can potentially share the spectrum with radar antennas, and joint operation is seen desirable and feasible in many application scenarios [7, 8]. Because antenna development can be both time-consuming and expensive, it is favorable to utilize developed antennas in several applications. With millimeter-wave antennas, this cost-effective approach is emphasized, due to the precision that is required in antenna design and manufacturing.

In this paper, we investigate the possibility of using phased-array antennas initially developed for 5G base-station applications in millimeter-wave image reconstruction. Thus, we are closing the gap between the communication and sensing antenna systems. An image-reconstruction method has been developed for this purpose, and it is an active one, meaning that the target space is illuminated with the imaging system. Active imaging is often seen as necessity to achieve sufficient dynamic range in the images [9]. Furthermore, the method relies on computational image forming. One of the well-known examples of computational imaging is synthetic aperture radars (SAR) [10].

Traditional phased-array imaging is done with a focused beam: the generated pencil-beam is used to scan the target space. This ultimately leads to a long measurement time even with the electrical beam-steering, because every pixel in the target space must be observed independently. The image-reconstruction time from the observed data can be short, since there is no need for multiple iterative rounds, but the overall time from the beginning of the observation to the final, formed image can be rather long.

---

*Received 1 December 2020, Accepted 7 February 2021, Scheduled 18 February 2021*

<sup>\*</sup> Corresponding author: Mikko K. Leino (mikko.k.leino@aalto.fi).

The authors are with the Department of Electronics and Nanoengineering, Aalto University School of Electrical Engineering, Aalto FI 00076, Finland.

Imaging with frequency-diverse system provides good alternative to achieve images quickly from the observed site [11]. The presented frequency-diverse imaging method utilizes scattered beams that illuminate the whole target space with much fewer beam patterns. This relies on measuring observations with frequency sweeps and allows much faster measurement time than with the traditional phased-array scanning. The image-reconstruction time from the sparse data can be the most time-consuming part of this method, but with properly chosen imaging scenes and optimized algorithms, the overall time can be greatly improved from that of the pencil-beam scanning method.

Recent years have seen interest in using frequency-diverse metasurfaces for imaging [11–14]. The main motivation has been to make imaging systems fast, planar, and low cost [11]. However, the beam patterns of the metasurface antennas can be quite unpredictable, and frequency-diverse metasurface systems are susceptible to alignment errors [15]. With phased arrays, we can achieve most of the aforementioned benefits in addition to the much better control over the beam-patterns, assuming that the phased array generates frequency-diverse beam patterns due to, e.g., a power division network. The beam diversity relies on the use of several beam patterns obtained using reconfigurable phased array, and the patterns can be optimized for different purposes without a need to redesign the whole antenna.

While it is undoubtedly true that many frequency-diverse imaging systems have lower costs than the phased arrays with active phase shifters, the industry is aiming for cheaper components and manufacturing prices due to the vast increase of the base-station antennas dictated by the 5G requirements. Hence, the possibility to use modern phased arrays in frequency-diverse millimeter imaging should also be researched. To the authors' knowledge, this paper presents the first realization where phased arrays designed for 5G communications are used in a frequency-diverse imaging application.

The rest of the paper is organized as follows: Section 2 introduces the image reconstruction method. Section 3 describes the measurement setup utilized for the imaging and the achieved results. Section 4 discusses the importance of these results and the future improvements. Finally, Section 5 concludes the paper.

## 2. IMAGING PROBLEM

The presented image-reconstruction method utilizes the frequency diversity of the antenna beam-patterns over the imaging band 24–32 GHz. The image is assumed to form as desired when there is enough variation in the target illumination. Multiple beam-patterns are further adopted to enhance this purpose. The imaging problem and method to reconstruct the image with frequency-diverse phased arrays have been previously discussed in [16], although only with simulations and at higher frequency. However, the problem formulation and signal model are valid for the presented system as well.

Figure 1 illustrates the problem setup and the concept of the presented imaging method. The method is driven by the idea that a large base-station antenna array can be divided to the subarrays, and each of them can have a different beam-pattern. Each subarray will sequentially illuminate the target space while the others operate in parallel to sample the reflected wave-front. The image is then formed computationally from the measured data. The principle is the same as, e.g., in [9], where the data acquisition is done with a multistatic sparse array, which compared to this work, has substantially more antenna elements.

The observations comprise the measured field strengths received from the target space. The signal model for a single observation  $y_{mn}$  at a frequency  $f_k$  for  $N$  voxels can be written as follows:

$$y_{mn}(f_k) = \sum_{i=1}^N (\mathbf{E}_n(\theta_i, \phi_i, f_k) \cdot \mathbf{E}_m(\theta_i, \phi_i, f_k)) \Gamma_i \frac{e^{-j \frac{4\pi f_k r_i}{c}}}{(4\pi r_i)^2}, \quad (1)$$

where  $\mathbf{E}_n$  denotes the illuminating electric field beam-pattern and  $\mathbf{E}_m$  the receiving one. Similarly,  $n$  indexes the transmitting pattern number and  $m$  the receiving one. Index  $k$  denotes the sampling frequency of the observation.

For the computational image-reconstruction, the target space is divided into voxels that are identified with index  $i$ .  $\theta_i$ ,  $\phi_i$ , and  $r_i$  describe the voxel location in the imaging system's field-of-view, and  $\Gamma_i$  denotes the reflection from the voxel, which is assumed to be zero if the voxel is empty and non-

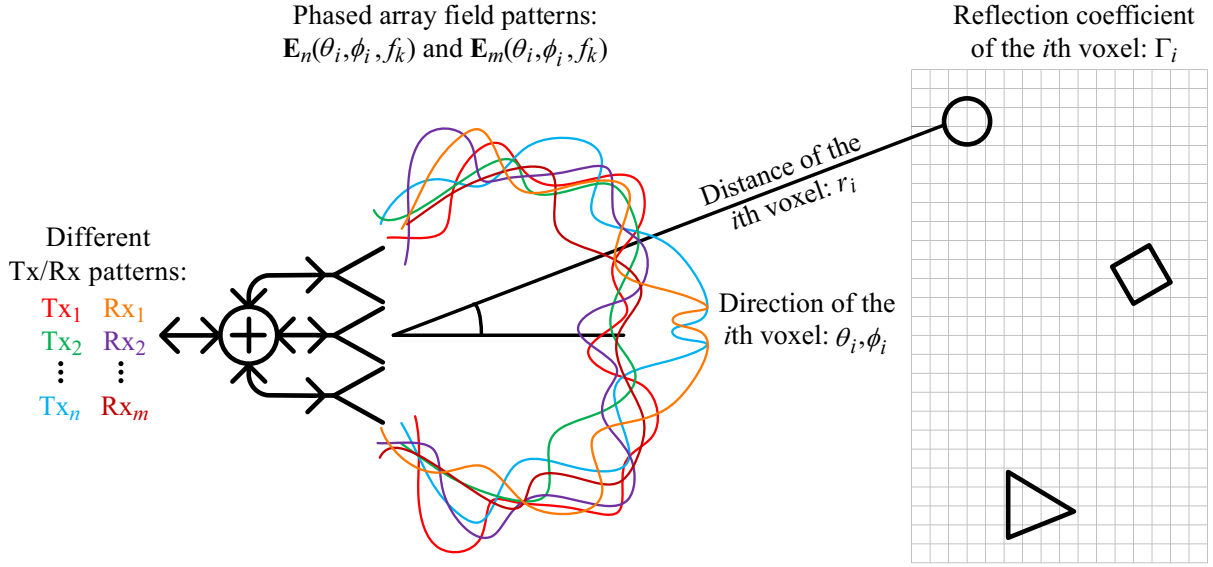


**Figure 1.** Frequency-diverse imaging method with phased arrays: a concept illustration.

zero if there is a target in the voxel. Reflections from targets are also assumed to be angle-independent and isotropic.

All measured observation data  $y_{mn}(f_k)$  are collected to the observation vector  $\mathbf{O}$ . The observation vector can be expressed as a product of the field data and target data as:

$$\mathbf{O}(y_{mn}(f_k)) = \mathbf{A}(P_{mn}(\theta_i, \phi_i, f_k), r_i)\mathbf{T}(\Gamma_i), \quad (2)$$

where  $\mathbf{T}$  is the vector containing the reflections, i.e., the target data over the target space  $(\theta_i, \phi_i, r_i)$ , and  $\mathbf{A}$  is the matrix containing the field data of different beam-pattern pairs  $P_{mn}(\theta_i, \phi_i, f_k)$  towards the target space:

$$P_{mn}(\theta_i, \phi_i, f_k) = \mathbf{E}_n(\theta_i, \phi_i, f_k) \cdot \mathbf{E}_m(\theta_i, \phi_i, f_k). \quad (3)$$

Even though the aforementioned equations are postulated for 3-D space, we only consider the imaging in 2-D in this paper, since our main interest is to take a straightforward approach and demonstrate that frequency-diverse imaging with phased arrays is possible in practice. Hence, index  $i$  denotes a pixel in the target space in the final algorithm.

In the simplest form, Eq. (2) could be rearranged as:

$$\mathbf{T} = \mathbf{A}^+\mathbf{O}, \quad (4)$$

with  $\mathbf{A}^+$  being the pseudo-inverse of the field-data matrix. The target vector  $\mathbf{T}$  would be then solved, and the result could be used to construct the image. However, the solution is not applicable in practice; for example, the model does not include noise or phase ambiguity that are present in the real-life measurements. They both disturb the image reconstruction, and hence, the data must be processed to acquire a sharp image.

### 3. IMAGING SETUP AND THE RESULTS

#### 3.1. Measurement Setup

An imaging system is built up to test the suggested imaging method in practice. The aim is to reconstruct images from the objects placed in the system's field-of-view. The system consists of two antennas presented in [5], originally designed for 5G backhauling. The antennas are  $4 \times 4$  phased arrays with square apertures of  $31.5 \times 31.5 \text{ mm}^2$ . The operation bandwidth  $B$  is 8 GHz, from 24 GHz to 32 GHz. Although not covered here, this bandwidth could theoretically allow range resolution of 19 mm:

$$\delta_r = \frac{c}{2B} = 19 \text{ mm}. \quad (5)$$

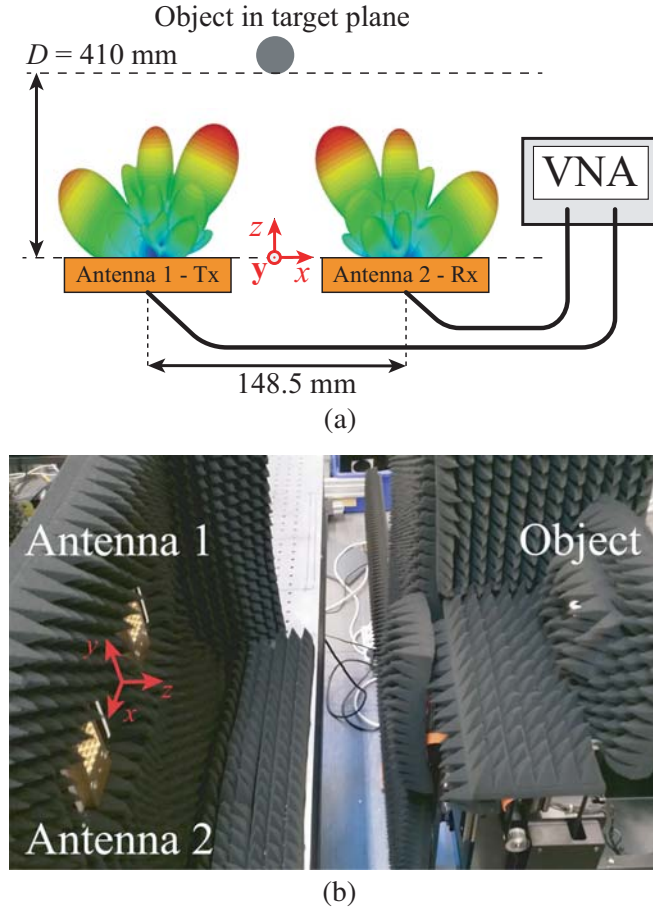


**Figure 2.** Image reconstruction setup: (a) Illustration of the setup. (b) Photograph of the imaging system setup.

The imaging system setup is illustrated in Fig. 2. Two antennas are utilized in the following way: the first antenna (Tx) illuminates the target, and the second antenna (Rx) records the reflected signal through a VNA. A computer is used to control the measurements and process the data. Spacing between the antennas is 148.5 mm. Target objects are located 41 cm from the imaging antennas, and they are placed on a sled normally used for probes in near-field antenna measurements. With the sled we can precisely control the location of the objects and test different target locations with relative ease. The width ( $x$  direction) and height ( $y$  direction) of the target plane are 75 cm and 50 cm, respectively, and the center of the plane is aligned with the point in the middle of the antennas.

The lateral resolution in the target space  $\delta_{cr}$  can be estimated by using the aperture sizes of the Tx and Rx antennas [9]:

$$\delta_{cr} = \frac{\lambda D}{L_t + L_r}, \quad (6)$$

where  $\lambda$  is the wavelength of the center frequency;  $D$  is the distance from the target plane to the antenna apertures; and  $L_t$  and  $L_r$  are the aperture sizes of the transmitting and receiving antennas, respectively. Since the two antennas have identical square apertures, the resolution estimations in  $x$  and  $y$  directions are the same. With  $L_t = L_r = 31.5$  mm, the lateral resolution estimation given by Eq. (6) is 70 mm. The same resolution estimation in both  $x$  and  $y$  directions might seem a bit counterintuitive at first, since the antennas are spatially separated in  $x$  direction. However, if one considers the obtainable resolution through the convolution of the transmitting and receiving antenna patterns, the spatial difference in either  $x$  or  $y$  direction does not matter as long as the beam patterns overlap with each other. The experimental results shown in the following sections indicate that this explanation is reasonable.

Furthermore, because we are interested in the capabilities of our imaging system, the target space is discretized with the size of 5 mm, roughly a half-wavelength at the center frequency. This results in  $151 \times 101$  pixels in the target space, and the phase shift for each pixel is calculated and included in the field-data matrix  $A$ .

The effect of the antenna beam patterns have been analyzed with simulations that utilize measurement data from both antennas: a measured response of each individual element. The simulated patterns correspond very well to the measured ones, and hence simulations can be certainly useful for analyzing the effect of the different patterns to the imaging algorithm and system. Based on the simulation studies, we have come to the conclusion that one antenna with six different patterns brings enough diversity to the system. This totals to 36 different beam-pattern pairs, which are acquired via 12 antenna-beam measurements. Individual antenna patterns are measured with the near-field scanner over the frequency band used in the image reconstruction, and the results are probe corrected. The field-pattern pairs are then calculated from the individual pattern results.

As an example, Fig. 3 shows the amplitude of one of the six selected patterns of antenna 1 in the target plane and one of the selected patterns for the antenna 2. The plots are labeled Tx and Rx, respectively, and below them the combination pattern of these two is illustrated. Frequency in these examples is 28 GHz, and the field patterns have been normalized to the plot-wise maximum values. It can be seen that the combination beam pattern leads to smaller detection areas in the target space. When we further consider the variety of different beam patterns and their frequency diversity, the whole target space can be imaged with good precision.

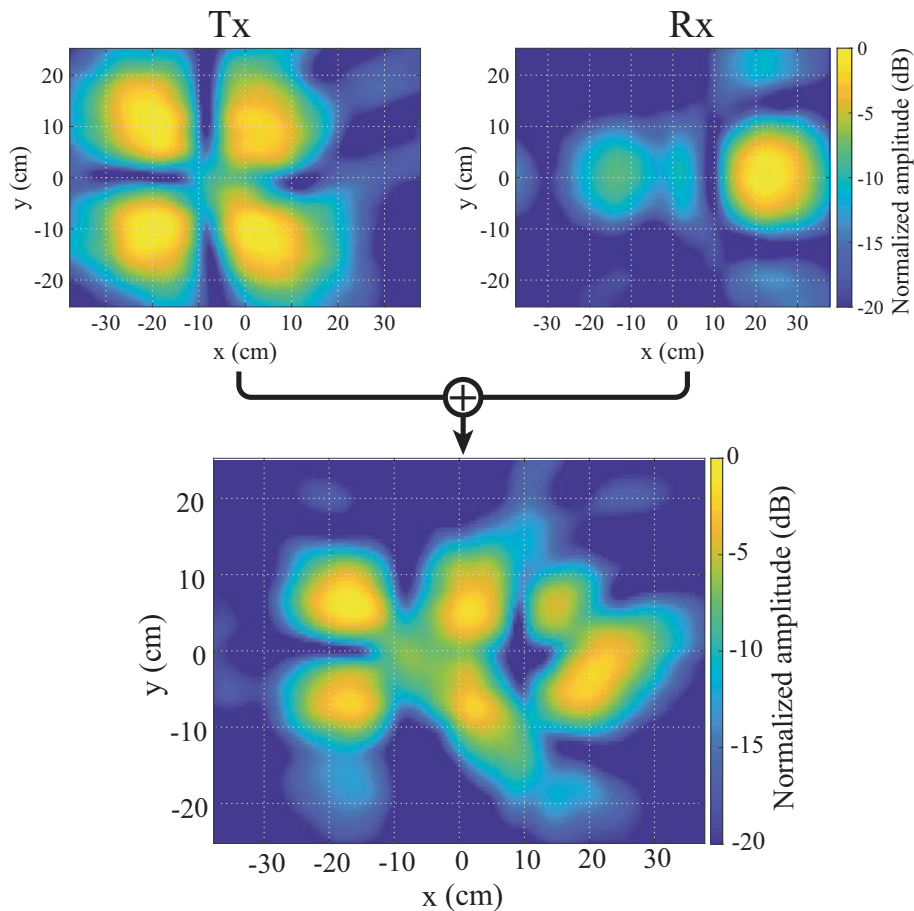


**Figure 3.** Example of the beam-pattern setup: Tx and Rx beam patterns are combined in the target space.

### 3.2. Data Processing

The measurement data processing is an essential step in the computational imaging. In the presented method, the measurement data are constructed from 161 frequency samples that are achieved with every 36 different patterns, thus, totaling 5796 observations. An image reconstruction algorithm has been constructed to form the image based on the measurement data. First, the free-space response of the target space without any objects is removed from the object measurements. Hence, we can remove the effect of mutual coupling between the imaging antennas and the reflections from the measurement setup that would distort the image.

Finally, the observation data are utilized to calculate the image via a linear inverse problem. We explored the possibility of forming the image by directly solving Eq. (4), but as described, the solution with real-life data is more complicated than in the ideal case. The noise and measurement uncertainties do not allow reconstruction of clear images. Hence, a different approach is taken, and the image is solved by using a least-square method and iterative algorithms. We have taken the inspiration from a two-step iterative shrinkage/thresholding algorithm (TwIST) [17], and we use its iterative algorithm along with the monotonicity requirement for the convergence. The algorithm has proven to be useful in several earlier microwave imaging studies at K-band [18–20], and because the proposed 5G antennas operate at  $K_a$ -band, the algorithm is a convenient choice here as well.

Furthermore, there is another difficulty due to the real-life implementation. The used near-field measurement setup does not allow the phase calibration, and hence, the absolute phase values of the imaging antennas are unknown, even though knowing them is essential for the current algorithm to work perfectly. Thus, only the amplitude patterns of the imaging antennas are considered in the algorithm while constructing the field-data matrix  $A$ . However, the phase terms due to the different propagation lengths back-and-forth to each pixel are still included in the matrix  $A$ , allowing the use of complex observation data. Nonetheless, the observation data have to be phase shifted so that the phase center for the observation is at the antenna aperture. Again, this is a crucial step for the algorithm to work properly.

To assert the quality of the imaging system, we have also calculated a singular value decomposition (SVD) curve from the different measurement modes, or more specifically, from the field data matrix  $A$ . The curve is normalized to its maximum value, and it is presented in Fig. 4 in logarithmic scale against the number of measurements. The steepness of the curve and the fact that it does not decay rapidly over the whole spectrum of measurements suggest that the field data and the corresponding frequency points provide frequency-diverse measurement data, as explained in [12].

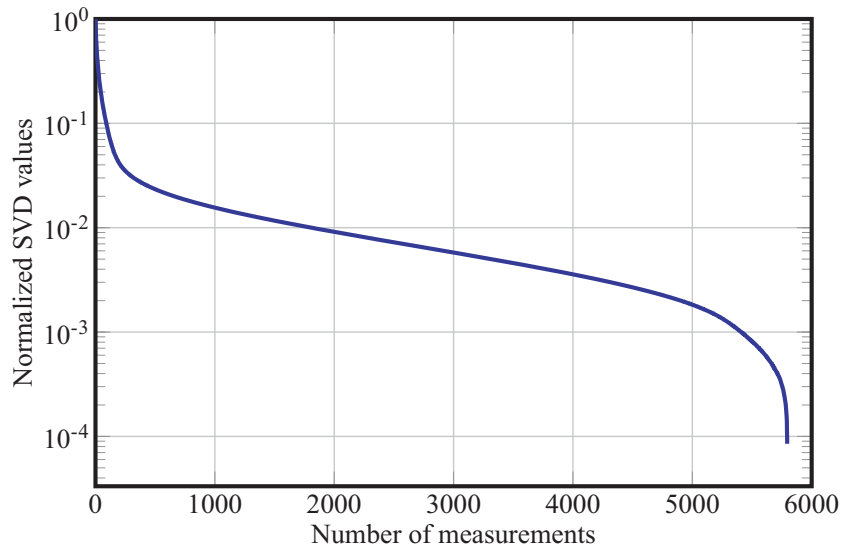


**Figure 4.** Singular value decomposition of the field data matrix  $A$ . Total number of measurements is 5796 and the SVD curve is normalized to its maximum value.

### 3.3. Image Results

Figure 5 shows a metallic sphere that is used as a target object in the imaging. The measured diameter of the sphere is 30 mm, which translates to  $2.4\text{--}3.2\lambda$  in 24–32 GHz band, thus making the ball a suitable test object, also, with respect to the expected cross-range resolution. Furthermore, the sphere is a well-known scatterer, who scatters the illumination over the whole solid angle, and hence, the sphere is easily traceable.



**Figure 5.** Picture of the sphere that is used as the target object.

Figure 6 presents the reconstructed images of the sphere in several locations of the target space. The actual locations, i.e., the sphere centers, are also marked. As seen from these images, the sphere can be found in different locations quite accurately, and the results are well within the cross-resolution estimations. The images are reconstructed in dB scale and normalized to the maximum response of the plot. The 3-dB width of the sphere's image averages around 60 mm in both  $x$  and  $y$  directions. The imaging method seems to make the targets appear larger in reconstructed images than what they are in reality. The probable explanation for this is the obtainable cross resolution, because the 3-dB width of 60 mm and calculated estimation of 70 mm are so close to each other.

The system works as intended, and the image reconstruction takes only a few seconds once the field-data matrix  $A$  is constructed beforehand. However, the system is still very sensitive for phase instability — for example, the aforementioned phase shift to the observation data appears to drift slightly depending on the target, and the variation can distort the image rather badly. Still, if we consider the resolution estimations with the current imaging system aperture, we manage to do quite well.

## 4. DISCUSSION

Obviously, the imaging results are heavily affected by the chosen antennas and constructed system. For example, the system has quite limited dynamic range and low SNR due to the low input power of the VNA. A more specifically constructed and optimized system could overcome some of the current problems, but the presented work shows already suitable results as a proof-of-concept: 5G base-station phased arrays are capable of frequency-diverse imaging. This finding certainly has many potential application scenarios. The images are acquired with good precision, and the reconstruction is fast. With further development and optimization, real-time imaging could be possible.

One major problem with the current system relates to the antenna phase and how it is utilized in the reconstruction algorithm. The current setup does not allow the use of the antenna phase, since

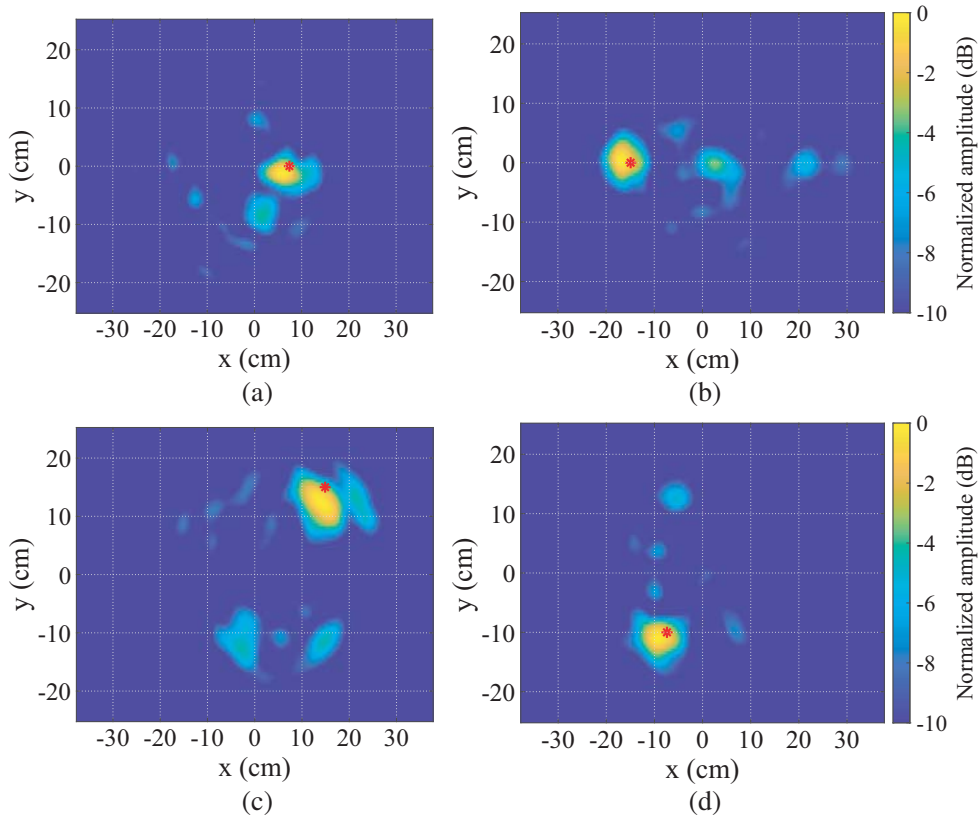


**Figure 6.** Reconstructed images of a metallic sphere in different locations (cm): (a)  $x = 7.4$ ;  $y = 0$ , (b)  $x = -14.9$ ;  $y = 0$ , (c)  $x = 14.9$ ;  $y = 15$ , and (d)  $x = -7.4$ ;  $y = -10$ . The red mark indicates the correct location of the sphere.

even a small phase uncertainty in the reconstruction algorithm leads to a severe ambiguity in the target location. This is a known problem in frequency-diverse imaging, and some phase calibration schemes have been presented [13]. Similar work should be also done for the presented system.

The imaging system could also benefit greatly from using neural networks in the measurement data processing for more accurate and efficient image reconstruction [21]. The optimal data acquisition itself has also many possible research directions that could be followed. As an example, the necessities for beam-patterns are still quite unknown: it is known that the patterns should provide enough dynamic range to the image construction, but more analytical or numerical approach could still be beneficial to make the image solving more efficient.

Diversity is also one of the issues that could be improved in the later studies. Now only one and same linear polarization is considered in both transmitting and receiving. The measurement of the cross-polarization could also potentially improve the image quality. Dual-polarized wide-band antennas capable of 5G communications like [22–24] could offer interesting options also as imaging antennas.

## 5. CONCLUSION

We have presented an experimental demonstration of the millimeter-wave imaging method that utilizes phased arrays whose main application is in 5G networks. Imaging proves to work for simple targets such as a metallic sphere, and the results are in line with our resolution estimations. Our work and progress in millimeter-wave imaging compare reasonably well with those utilizing, e.g., frequency-diverse metasurfaces.

However, further studies should be performed, although this work serves as a proof-of-concept. There are many potential research directions: obtain better understanding of the requirements for the

different beam-patterns, develop the reconstruction algorithm further, and investigate the possibility of using neural networks in the image reconstruction. In addition, imaging should be expanded in 3D to take into account the range component as well, and imaging system capabilities could be further investigated in a separate resolution study with proper resolution targets.

## ACKNOWLEDGMENT

The work of M. K. Leino was supported in part by the Walter Ahlström Foundation, the Jenny and Antti Wihuri Foundation, and the Nokia Foundation.

## REFERENCES

1. Gu, X., A. Valdes-Garcia, A. Natarajan, B. Sadhu, D. Liu, and S. K. Reynolds, "W-band scalable phased arrays for imaging and communications," *IEEE Communications Magazine*, Vol. 53, No. 4, 196–204, Apr. 2015.
2. Eudeline, P., "Survey of active electronically scanned antenna in Thales radars," *2013 IEEE International Symposium on Phased Array Systems and Technology*, 12–16, Waltham, USA, Oct. 2013.
3. Agrawal, A. K. and E. L. Holzman, "Beamformer architectures for active phased-array radar antennas," *IEEE Transactions on Antennas and Propagation*, Vol. 47, No. 3, 432–442, Mar. 1999.
4. Kibaroglu, K., M. Sayginer, T. Phelps, and G. M. Rebeiz, "A 64-element 28-GHz phased-array transceiver with 52-dBm EIRP and 8-12-Gb/s 5G link at 300 meters without any calibration," *IEEE Transactions on Microwave Theory and Techniques*, Vol. 66, No. 12, 5796–5811, Dec. 2018.
5. Leino, M. K., R. Montoya Moreno, J. Ala-Laurinaho, R. Valkonen, and V. Viikari, "Waveguide-based phased array with integrated element-specific electronics for 28 GHz," *IEEE Access*, Vol. 7, 90 045–90 054, 2019.
6. Kuai, L., J. Chen, Z. H. Jiang, C. Yu, C. Guo, Y. Yu, H. Zhou, and W. Hong, "A N260 band 64 channel millimeter wave full-digital multi-beam array for 5G massive MIMO applications," *IEEE Access*, Vol. 8, 47 640–47 653, 2020.
7. Guan, J., A. Paidimarri, A. Valdes-Garcia, and B. Sadhu, "3D imaging using mmWave 5G signals," *2020 IEEE Radio Frequency Integrated Circuits Symposium (RFIC)*, 147–150, Los Angeles, USA, Aug. 2020.
8. Liu, F., C. Masouros, A. P. Petropulu, H. Griffiths, and L. Hanzo, "Joint radar and communication design: Applications, state-of-the-art, and the road ahead," *IEEE Transactions on Communications*, Vol. 68, No. 6, 3834–3862, Jun. 2020.
9. Ahmed, S. S., A. Schiessl, and L. Schmidt, "A novel fully electronic active real-time imager based on a planar multistatic sparse array," *IEEE Transactions on Microwave Theory and Techniques*, Vol. 59, No. 12, 3567–3576, Dec. 2011.
10. Moreira, A., P. Prats-Iraola, M. Younis, G. Krieger, I. Hajnsek, and K. P. Papathanassiou, "A tutorial on synthetic aperture radar," *IEEE Geoscience and Remote Sensing Magazine*, Vol. 1, No. 1, 6–43, Mar. 2013.
11. Imani, M. F., J. N. Gollub, O. Yurduseven, A. V. Diebold, M. Boyarsky, T. Fromenteze, L. Pulido-Mancera, T. Slesman, and D. R. Smith, "Review of metasurface antennas for computational microwave imaging," *IEEE Transactions on Antennas and Propagation*, Vol. 68, No. 3, 1860–1875, Mar. 2020.
12. Zvolensky, T., V. R. Gowda, J. Gollub, D. L. Marks, and D. R. Smith, "W-band sparse imaging system using frequency diverse cavity-fed metasurface antennas," *IEEE Access*, Vol. 6, 73 659–73 668, 2018.
13. Yurduseven, O., T. Fromenteze, and D. R. Smith, "Relaxation of alignment errors and phase calibration in computational frequency-diverse imaging using phase retrieval," *IEEE Access*, Vol. 6, 14 884–14 894, 2018.

14. Yurduseven, O., T. Fromenteze, D. L. Marks, J. N. Gollub, and D. R. Smith, "Frequency-diverse computational microwave phaseless imaging," *IEEE Antennas and Wireless Propagation Letters*, Vol. 16, 2808–2811, 2017.
15. Odabasi, H., M. Imani, G. Lipworth, J. Gollub, and D. Smith, "Investigation of alignment errors on multi-static microwave imaging based on frequency-diverse metamaterial apertures," *Progress In Electromagnetics Research B*, Vol. 70, 101–112, 2016.
16. Leino, M. K., J. Ala-Laurinaho, Z. Purisha, S. Särkkä, and V. Viikari, "Millimeter-wave imaging method based on frequency-diverse subarrays," *2019 12th Global Symposium on Millimeter Waves (GSMM)*, 84–86, Sendai, Japan, May 2019.
17. Bioucas-Dias, J. M. and M. A. T. Figueiredo, "A new TwIST: Two-step iterative shrinkage/thresholding algorithms for image restoration," *IEEE Transactions on Image Processing*, Vol. 16, No. 12, 2992–3004, Dec. 2007.
18. Yurduseven, O., M. F. Imani, H. Odabasi, J. Gollub, G. Lipworth, A. Rose, and D. R. Smith, "Resolution of the frequency diverse metamaterial aperture imager," *Progress In Electromagnetics Research*, Vol. 150, 97–107, 2015.
19. Lipworth, G., A. Mrozack, J. Hunt, D. L. Marks, T. Driscoll, D. Brady, and D. R. Smith, "Metamaterial apertures for coherent computational imaging on the physical layer," *Journal of the Optical Society of America A*, Vol. 30, No. 8, 1603–1612, Aug. 2013.
20. Zhu, R., T. Zvolensky, and D. Marks, "Millimeter wave computational imaging with 3D printed leaky wave frequency diverse antenna," *2016 41st International Conference on Infrared, Millimeter, and Terahertz waves (IRMMW-THz)*, 1–1, Copenhagen, Denmark, Sep. 2016.
21. Tamminen, A., S.-V. Pälli, J. Ala-Laurinaho, A. Aspelin, A. Oinaanoja, and Z. Taylor, "Holograms with neural-network backend for submillimeter-wave beamforming applications," *Proc. SPIE*, Vol. 11411, 10 pages, Online Only, Apr. 2020.
22. Gu, X., D. Liu, C. Baks, O. Tageman, B. Sadhu, J. Hallin, L. Rexberg, P. Parida, Y. Kwark, and A. Valdes-Garcia, "Development, implementation, and characterization of a 64-element dualpolarized phased-array antenna module for 28-GHz high-speed data communications," *IEEE Transactions on Microwave Theory and Techniques*, Vol. 67, No. 7, 2975–2984, Jul. 2019.
23. Kähkönen, H., J. Ala-Laurinaho, and V. Viikari, "Dual-polarized Ka-band Vivaldi antenna array," *IEEE Transactions on Antennas and Propagation*, Vol. 68, No. 4, 2675–2683, Apr. 2020.
24. Nafe, A., M. Sayginer, K. Kibaroglu, and G. M. Rebeiz, " $2 \times 64$ -element dual-polarized dual-beam single-aperture 28-GHz phased array with  $2 \times 30$  Gb/s links for 5G polarization MIMO," *IEEE Transactions on Microwave Theory and Techniques*, Vol. 68, No. 9, 3872–3884, Sep. 2020.